



## Modeling the impact of wildfire on air quality in Nepal using WRF-Chem and Sentinel-5P

Kundan Lal Shrestha <sup>a</sup>\*, Aakriti Gyawali <sup>b</sup>, Sabina Gyawali <sup>b</sup>, Prayon Joshi <sup>c</sup>, Subodh Sharma <sup>b,c,\*</sup>

<sup>a</sup> Department of Chemical Science and Engineering, School of Engineering, Kathmandu University, Dhulikhel, Kavre, Nepal

<sup>b</sup> Department of Environmental Science and Engineering, School of Science, Kathmandu University, Dhulikhel, Kavre, Nepal

<sup>c</sup> Aquatic Ecology Centre, School of Science, Kathmandu University, Dhulikhel, Kavre, Nepal

### ARTICLE INFO

#### Keywords:

Fire emissions  
Remote sensing  
Aerosols  
Chemical transport

### ABSTRACT

Nepal is prone to wildfires, which contribute significantly to air pollution during the dry seasons. We studied a series of such wildfire events in Nepal occurring from November 2020 to April 2021. Along with the simulation in the WRF-Chem model, we used Sentinel-5P satellite data for analyzing pollutants during excessive fire events in Nepal. Comparison was done between the concentration obtained from numerical modeling with the satellite observation. Simulation was done for December 2021 using the Fire Inventory from NCAR (FINN) fire emissions dataset, and other anthropogenic emission data. Maximum fire contribution in December 2020 was about 120% increase in NO<sub>2</sub>, 48% in PM<sub>2.5</sub>, 35% in PM<sub>10</sub>, 32% in CO, 28% in SO<sub>2</sub>, and 17.5% in NH<sub>3</sub>. Winter season (November–February) had a low fire count but the pre-monsoon season (March–April) had a high fire count in Nepal. Wildfires contributed to high levels of pollution during March and April 2021, due to high fire counts where maximum UV-AAI was 0.8315, and CO and NO<sub>2</sub> column number density were 0.067 mol m<sup>-2</sup> and 4.1204 × 10<sup>-5</sup> mol m<sup>-2</sup> respectively. The ground station measured peak PM<sub>2.5</sub> concentration in Kathmandu Valley of 270 µg m<sup>-3</sup>. Comparison between the WRF-Chem and Sentinel-5P results showed strong correlation ( $r > 0.8$ ) for NO<sub>2</sub> and CO. The ground station data also suggests a severe decline in air quality due to the wildfire events (2020–2021) in Nepal. Thus, urgent need for stronger policies and their implementation is needed. Similar integrated studies can be undertaken for data-driven decision-making to identify the wildfire hotspots and their contribution toward the emission and transport of air pollutants.

### 1. Introduction

Wildfires are one of the major sources of gaseous and particle pollution in the atmosphere. The increase in average PM<sub>10</sub> and PM<sub>2.5</sub> concentration, organic aerosol mass, and gaseous concentrations of many pollutants, including carbon monoxide (CO), ozone (O<sub>3</sub>), nitrogen oxides (NO<sub>x</sub>), sulfur dioxide (SO<sub>2</sub>) and ammonia (NH<sub>3</sub>), can be a consequence of forest fire emissions (Lazaridis et al., 2008). Wildfire pollutants that are transported can cause severe exposure to humans who are far from the fire (Crippa et al., 2016). Humans are frequently responsible for wildfires, whether on purpose or by accident. People often set forests on fire to make charcoal, to startle animals out of the shelter for hunting, or to clear forests in the hopes of fostering the growth of new grass flushes (Reuters, 2021).

From previous studies, it is known that the most affected air quality parameters due to the wildfires are aerosols (Sadavarte et al., 2019;

Fatholahi et al., 2020), NOx (Menon et al., 2007), SO<sub>2</sub> (Ukhov et al., 2020), CO and CH<sub>4</sub> (Magro et al., 2021).

The Himalayan region with fragile ecosystem, an important storehouse of freshwater reserves has been increasingly threatened by climate change, pollution and wildfires. Biomass burning, particularly along the Himalayan foothills and Southeast Asia, has emerged as a major source of black carbon (BC) emissions, which are transported to the Tibetan Plateau and deposited on glaciers, accelerating snowmelt and altering regional hydrology (Xu et al., 2018). Simultaneously, forest fires in the Western Himalayas, including regions like Uttarakhand, Himachal Pradesh, and Jammu and Kashmir, have been linked to significant increases in atmospheric pollutants such as CO, NO<sub>2</sub>, SO<sub>2</sub>, formaldehyde, and aerosols, which have deteriorated the air quality of the region (Murmu et al., 2022). In the broader Hindu Kush Himalayan region, forest fires which was primarily human induced showcased a

\* Corresponding authors.

E-mail addresses: [kundan@ku.edu.np](mailto:kundan@ku.edu.np) (K.L. Shrestha), [aakritigyawali766@gmail.com](mailto:aakritigyawali766@gmail.com) (A. Gyawali), [sabinaagyawali@gmail.com](mailto:sabinaagyawali@gmail.com) (S. Gyawali), [prayonjoshi@gmail.com](mailto:prayonjoshi@gmail.com) (P. Joshi), [subodh.sharma@ku.edu.np](mailto:subodh.sharma@ku.edu.np) (S. Sharma).

strong association with increased aerosol optical depth (AOD) and CO concentrations, demonstrating their severe impact on air quality (Bhattarai et al., 2022). Himalayas act as both a barrier and a channel for the spread of wildfire related aerosols and gases. Hence, understanding wildfire impacts in this region is critical for evaluating transboundary air pollution effects.

Nepal is a landlocked country in South Asia situated mainly in the foothills of the Himalayas. Nepal was ranked 12th out of 106 countries in the world for worst air quality in 2020 with an average Air Quality Index (AQI) of 110 (IQAir, 2021). Nepal contains a diverse spectrum of geographical landscapes, including numerous mountain ranges and lowlands that help to raise the country's existing high pollution levels by creating pollution sinks (IQAir, 2021). The major causes of air pollution in Nepal are vehicular emissions, industrial emissions, open burning, wildfires, etc.

Along with these pollutants, wildfire events are also the main source of aerosols, mainly between November to March (Parajuli et al., 2015). In the year 2021, the wildfire events were higher in number than the previous years. A series of wildfires that started on November 15, 2020, to April 2021 caused a tremendous disaster and dropped air quality to hazardous levels in Nepal. Around 2700 forest fires throughout 73 out of 77 districts were recorded (Jamwal, 2021). The main reason attributed to high-intensity wildfire events was the decrease in precipitation level that increased the dryness in forest, resulting in wildfires (DHM, 2021).

WRF-Chem, Weather Research and Forecasting Model coupled with chemistry, is suitable for studying the feedback between chemistry and meteorology for air quality forecasting on regional to cloud-resolving scales (Grell et al., 2011). The WRF-Chem enables researchers to understand the movement of smoke particulates, which helps to understand the impact of forest fires, and biomass burning on the given domain (Mues et al., 2017; Shi et al., 2019; Xu et al., 2018). Satellite imagery, such as Copernicus Sentinel 5-P is also widely used for the study of air pollutants.

Several global and regional studies have analyzed the effect of wildfires on air quality. For instance, Shi et al. (2019) investigated record-breaking wildfires in Southern California using the WRF-Chem model and reported that wildfire events accounted for 14–42% of total PM<sub>2.5</sub> exposure, significantly affecting air quality and human health. Zhu et al. (2018) simulated and investigated the transport of smoke aerosol and quantification of impacts of wildfire in Russia using MODIS data. Several wildfires were observed across Siberia during the period of 18–27 July 2016. The forest fires had a wide range of effects on air quality affecting Central Asia, Mongolia, and Northern China (Zhu et al., 2018). Magro et al. (2021) studied atmospheric trends of CO and CH<sub>4</sub> from wildfires in Portugal using Sentinel-5P TROPOMI (TROPOspheric Monitoring Instrument) Level-2 Data. CO and methane (CH<sub>4</sub>) spatial distribution and trend were studied prior, during and after the devastating fire events (2018–2019) in Portugal. Fatholah et al. (2020) estimated the PM<sub>2.5</sub> concentration during the wildfire season in British Columbia, Canada using satellite optical data and geographically weighted regression (GWR) model. Higher PM<sub>2.5</sub> concentration was found during the wildfire season (Fatholah et al., 2020).

In Nepal, wildfire-related studies have also been conducted using satellite datasets. Parajuli et al. (2015) examined the spatial and temporal distribution of wildfires from 2000 to 2013 using MODIS active fire data, identifying 30,220 hotspots, primarily during the hot and dry season where most of the wildfire occurred in the Himalayan region (Parajuli et al., 2015). Recent studies have examined the impact of wildfires on air quality in the Kathmandu Valley. A case study of the March–April 2021 forest fire events revealed significant increases in PM<sub>2.5</sub> concentrations, reaching maximum levels of 371 µg/m<sup>3</sup> during the first fire episode and 280 µg/m<sup>3</sup> during the second fire event (Khadgi et al., 2024). Another study on air quality in the Kathmandu Valley from 2018 to 2022 identified 47 days where the

daily PM<sub>2.5</sub> limit of 100 µg/m<sup>3</sup> was exceeded, with maximum pollution level of 305 µg/m<sup>3</sup>. The pollution was mainly attributed to wildfire, and the pollution highly correlated with fire counts (Kuikel et al., 2024). These findings demonstrate the need for detailed atmospheric modeling to capture the transport and dispersion of wildfire-related pollutants. Hence, while there have been studies regarding the effect of wildfires previously, only a few studies are available on the fate of the pollutants arising and being transported from the wildfires. Hence, we studied the pollutants emitted from the series of wildfire events and their transportation using WRF-Chem modeling and Sentinel 5-P satellite imagery. We then compared the air pollutant concentrations from the WRF-Chem model with those from Sentinel-5P.

## 2. Methods

Our analysis focus on the entire region of the country Nepal, covering an area of 1,47,181 km<sup>2</sup>. Nepal stretches by 880 km along its east–west axis and on north–south axis by 150 to 250 km (Fig. 1.). Population of Nepal is 29,842,045, and the capital city Kathmandu has 2041,587 population with a high population density of 5169 persons per km<sup>2</sup> (NPHC, 2021). Besides the capital city, population is high in the Terai region.

Summer temperature of Nepal ranges from 28 °C to 40 °C and average maximum and minimum temperature of Nepal is often below the freezing point to 23 °C in winter. Nepal's topography is divided into three main regions: lowland Terai, Hilly region, and Himalayas, ranging in elevation from 60 m to 8848 m (Bhattarai et al., 2022). Traditionally there are six seasons, but narrowing down, Nepal has summer (pre monsoon), monsoon and winter (post monsoon) season with climate variation largely influenced by altitude and the South Asian monsoon (Bista, 2019; Yang et al., 2017). Annual rainfall ranges from 1500 mm to 2500 mm, primarily during the monsoon (June–September) (Karki et al., 2017). The winter season of Nepal is usually dry with a very low level of precipitation, i.e., 20–25 mm.

### 2.1. WRF-Chem model

WRF-Chem is an online Weather Research and Forecasting Model coupled with chemistry. WRF-Chem model uses chemistry and meteorology for simulation of the emission as well as the fate of these trace gases after emission and aerosols, which can be used to estimate regional air quality and interaction between cloud and chemistry. This model can be used to access the impact of wildfire on air quality. For generating emission of wildfire by using WRF-Chem, anthropogenic, biogenic, fire emissions, boundary conditions, and different pre-processors were used. For setting up the model we used the Mercator projection system, with a grid resolution of 15 km × 15 km (Fig. S1). The number of grid cells was 64 × 60 cells, with 42 vertical layers.

#### 2.1.1. Initial, boundary conditions, and emission data sets

The initial and lateral boundary conditions for meteorological data were derived from ERA-5 Reanalysis data. It consists of 137 vertical layers from the ground surface with spatial resolution of 31 km.

The geographical input data were obtained from UCAR (University Corporation for Atmospheric Research).

For the chemical boundary conditions, CAM-CHEM version 4 data was used. CAM-CHEM is a component of NCAR and an implementation of chemistry with the Community Earth System Model (CESM). The conventional tropospheric chemical mechanism implemented within the CESM CAM-CHEM structure is the Model for Ozone and Related Chemical Tracers, version 4 (MOZART-4) mechanism.

The anthropogenic emission was obtained from Emission Database for Global Atmospheric Research (EDGAR HTAP V2) inventory. It is a top-down compilation of annual and monthly grid maps of anthropogenic air pollution emissions (with a grid resolution of 0.1 degree

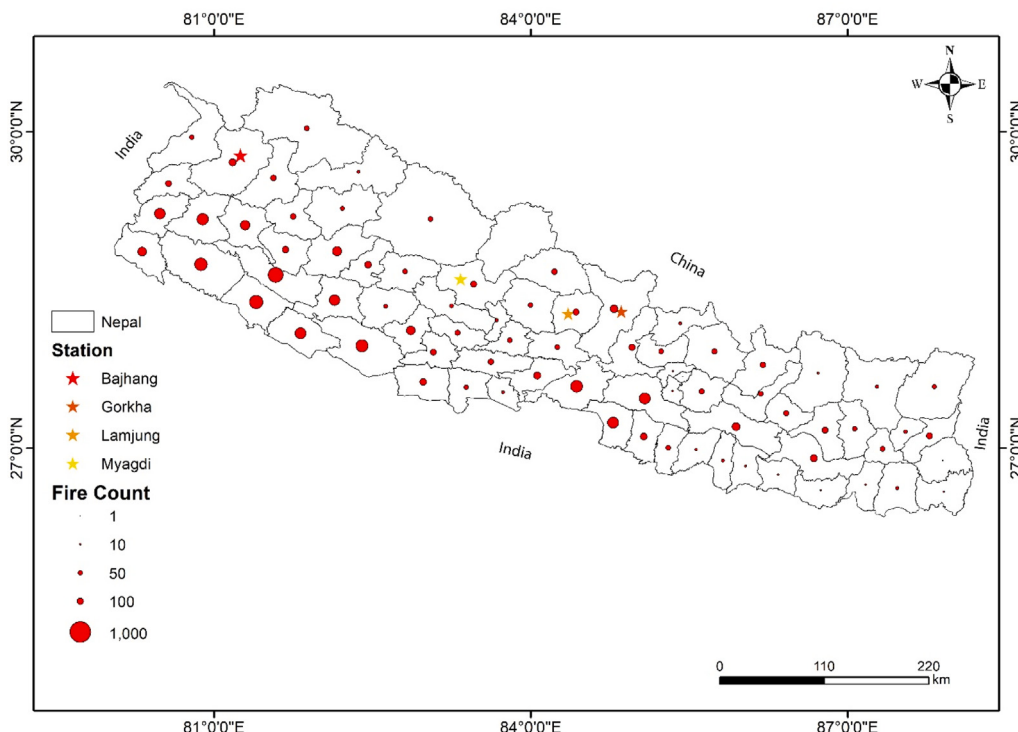


**Fig. 1.** District level map of Nepal showing the fire count from November, 2020 to April, 2021 (obtained from MODIS) as well as four stations for investigation of air pollutant concentration from WRF-Chem.

$\times 0.1$  degree) inventory calculated using activity data and emission factors. It contains annual inventories for gases CH<sub>4</sub>, NMVOC, CO, SO<sub>2</sub>, NO<sub>x</sub>, NH<sub>3</sub>, PM<sub>10</sub>, PM<sub>2.5</sub>, BC, and OC (Janssens-Maenhout et al., 2012).

The biogenic emission was obtained from Model of Gases and Aerosols from Nature (MEGAN). It is an offline model for biogenic emission having a base resolution of about 1 km and can be coupled with land surface and atmospheric chemistry models (Guenther et al., 2006). It consists of the sum of monthly emission of gases that occurs naturally except biomass burning and animal feedlots.

For biomass burning data, Fire Inventory from the National Centre for Atmospheric Research (NCAR) (FINN) version 1.5 was used. It provides global emission of trace gases and particles from open burning of biomass containing wildfire, agricultural fire, and prescribed burning but doesn't include the use of biofuel and trash burning (Jena et al., 2015).

### 2.1.2. Simulation

For model simulations, Weather Research and Forecasting model coupled with chemistry (WRF-Chem) version 4.3 was used. The simulation covered the period from 1 December 2020 to 30 December 2020. Simulation of the model was done for the domain covering overall Nepal and certain parts of India and China as well. We couldn't carry out the simulation for the time period of March–April, 2021 due to the unavailability of input data (FINN emission) for the year 2021. The list of physics and chemistry options used in the model is given in Table 1.

For Chemistry parameterization, MOZART chemistry with Global Ozone Chemistry Aerosol Radiation and Transport (GOCART) aerosol (MOZCART) with Madronich F-TUV photolysis was used. GOCART was developed to simulate the distribution of sulfur species in the atmosphere. The model solves the continuity equation that contains emission, chemistry, advection, convection, diffusion, dry deposition, and wet deposition of each species.

### 2.1.3. Post-processing

The output from the WRF model can be handled from numerous points of view. Tools like NCL, Vapor, and RIP can be used to handle

information. In our research netCDF4 files were obtained for the emission of 7 different species, namely PM<sub>10</sub>, PM<sub>2.5</sub>, NO<sub>2</sub>, CO, SO<sub>2</sub>, NH<sub>3</sub>, and O<sub>3</sub>, in both fire and non-fire conditions. The files were analyzed in Python 3.0 with netCDF4 for analyzing the output files, and Matplotlib package for visualization.

The contribution of wildfire on pollutant concentration was calculated using Eq. (1). It represents the percent amount of pollutant that increases due to wildfire with respect to the pollutant concentration when wildfire is absent.

$$\% \text{ Contribution of wildfire} = \frac{(Fire - Nofire)}{Nofire} \times 100\% \quad (1)$$

where:

*Fire* : Air pollutant concentration using WRF-Chem with wildfire emissions.

*Nofire* : Air pollutant concentration using WRF-Chem without wildfire emissions.

### 2.2. Satellite imagery

Nepal's intended spatial domain extends from 28°00'N latitude to 84°00'E longitude. The monthly variance across Nepal was determined using the Sentinel-5P TROPOMI dataset from November 2020 to April 2021. The Google Earth Engine (GEE) platform was utilized in the analysis and data generation of various products, including those from the Sentinel-5P satellite's TROPOMI sensor.

The species selected from the satellite image for analysis and their information are provided in Table S1.

The JavaScript editor, which is part of the Google Earth Engine (GEE) Code Editor Developer framework, was used to analyze all of the variables. To acquire a full perspective of emission variation from wildfire of all the relevant trace gases in the atmosphere, the available offline data was used, and a 6-months variation of five air quality indicators were analyzed.

**Table 1**  
Physics and chemistry parameters selected for running WRF-Chem model.

Parameters	Options
<b>Physics options</b>	
Microphysics	WSM 5-class scheme
Cumulus	Grell 3-D
Longwave	RRTMG (Rapid Radiative Transfer Model)
Shortwave	Dudhia shortwave scheme
Planetary boundary layer	Younsei University PBL
Land surface	MYJ
<b>Chemistry options</b>	
Chemistry scheme	MOZCART chemistry with GOCART aerosols (MOZCART) using KPP library
Photolysis option	Madronich F-TUV photolysis
Biogenic option	MEGAN biogenic emission online based upon weather, land use data
Fire emissions	FINN, MOZART -4
Aerosol	GOCART
Background emission	GOCART background data
Aerosol optical properties	Calculation based upon volume

Fire hotspots were obtained from MODIS collection 6 active fire datasets (Giglio et al., 2016). The active fire location provided by MODIS signifies the center of a 1 km pixel that is marked by the algorithm as containing one or more fires within the pixel.

The WRF-Chem output was validated with the Sentinel-5P tropospheric column density (Yarragunta et al., 2025). The modeled outputs from WRF-Chem were compared against Sentinel-5P satellite retrievals for two key atmospheric pollutants: nitrogen dioxide ( $\text{NO}_2$ ) and carbon monoxide (CO). This comparison was carried out for the entire month of December 2020.

The comparison process involved aligning both the horizontal and vertical grids of the two datasets. For  $\text{NO}_2$ , the modeled vertical concentration profiles from WRF were first interpolated to match the pressure levels of Sentinel-5P. These were then multiplied using the satellite's Averaging Kernel (AK) to obtain a satellite-comparable retrieval profile (Yarragunta et al., 2025). The resulting vertically weighted  $\text{NO}_2$  profiles from WRF were vertically integrated to derive total column concentrations, which were then directly compared with the tropospheric column concentrations from Sentinel-5P using various metrics (Eqs. (2), (3), (4), and (5)). These metrics provided the performance of WRF-Chem in comparison to the data derived from satellite images.

$$RMSE = \sqrt{\frac{1}{n} \sum_{i=1}^n (y_i - x_i)^2} \quad (2)$$

$$MAE = \frac{1}{n} \sum_{i=1}^n |y_i - x_i| \quad (3)$$

$$MB = \frac{1}{n} \sum_{i=1}^n (y_i - x_i) \quad (4)$$

$$r = \frac{\sum_{i=1}^n (x_i - \bar{x})(y_i - \bar{y})}{\sqrt{\sum_{i=1}^n (x_i - \bar{x})^2} \sqrt{\sum_{i=1}^n (y_i - \bar{y})^2}} \quad (5)$$

where:

y: WRF-Chem data

x: Sentinel-5P data

n: number of data

### 2.3. Ground observation

The  $\text{PM}_{2.5}$  data for this study was obtained from US-Embassy, Phora Durbar Kathmandu station <https://np.usembassy.gov/air-quality-monitor/> for March and April 2021.

## 3. Results and discussion

### 3.1. WRF-Chem

Fire hotspot data for the domain was extracted from Fire Information for Resource Management System (FIRMS) database for the study period. Fig. S3 shows active hotspots for December 2020 within the domain. The fire mostly occurred in hilly and mountainous regions of Nepal, and major hotspots were located in the districts such as Gorkha, Lamjung, Myagdi, and Bajhang. Northern India also had large fire events during the study period. Fig. 2 shows daily active fire counts during November, 2020 to April, 2021. The counts in March–April is quite high in comparison to other months. In another study it has been found that the incidence of wildfire and the area affected shows an increasing trend over 17 years (2000–2016) (Bhujel et al., 2017). In 2016, the area coverage by the wildfire increased by 42% while the wildfire incidence increased by around 33% than previous years (2000–2016) (Bhujel et al., 2017).

Wildfires increase the polluting gases and aerosols in the atmosphere. In Nepal, the Hill Sal forest covers the most area and also contributes in the highest carbon emission in the form of CO,  $\text{CH}_4$ , and  $\text{CO}_2$  during the wildfire events (Bhujel et al., 2020). The wildfires also contributes in the increasing level of  $\text{PM}_{2.5}$  concentration (McClure and Jaffe, 2018),  $\text{NO}_x$  and  $\text{O}_3$  (Val Martín et al., 2006), etc.

The percentage contribution of wildfires in air pollutants CO,  $\text{NH}_3$ ,  $\text{NO}_2$ ,  $\text{SO}_2$ ,  $\text{PM}_{10}$ , and  $\text{PM}_{2.5}$  is shown in Fig. S2. Maximum fire contribution was about 120% increase in  $\text{NO}_2$ , 48% in  $\text{PM}_{2.5}$ , 35% in  $\text{PM}_{10}$ , 32% in CO, 28% in  $\text{SO}_2$ , and 17.5% in  $\text{NH}_3$ . In Fig. 3, we can see that the maximum contribution of wildfire on air pollutants represented by dark red area was mostly located in Gorkha and Lamjung districts of Nepal with maximum fire hotspots. Both the Gorkha and Lamjung are in similar latitude whereas the Bajhang and Myagdi lies further north. There was a huge contribution of wildfire to  $\text{NO}_2$ . From the images, distinct pollutants plumes from a wildfire can be observed originating from Gorkha, Lamjung and Bajhang district of Nepal (Fig. 3). The pollutants were dispersed and transported from the originating area. Pollutants like  $\text{NH}_3$ ,  $\text{SO}_2$ ,  $\text{PM}_{10}$  and  $\text{PM}_{2.5}$  were transported to wider area of Tibetan region and had caused higher effect on air quality of China whereas CO had more effect inside Nepal and near the hotspots rather than in the Tibetan region. In India, maximum contributions of fire on air pollutants were located in Uttar Pradesh and Bihar region with maximum hotspots, which also had effect on air quality in Nepal. Fire event in Nepal seemingly had effects on Tibetan region of China which can be mainly due to transport of wildfire plumes by wind. Also, the fire events in India had an effect on the air quality of Nepal. There was significant effect on air quality in the overall domain from wildfire. The spatial images gave us general idea about the fate, transport, and the contribution of wildfire to air quality parameters during the study period.

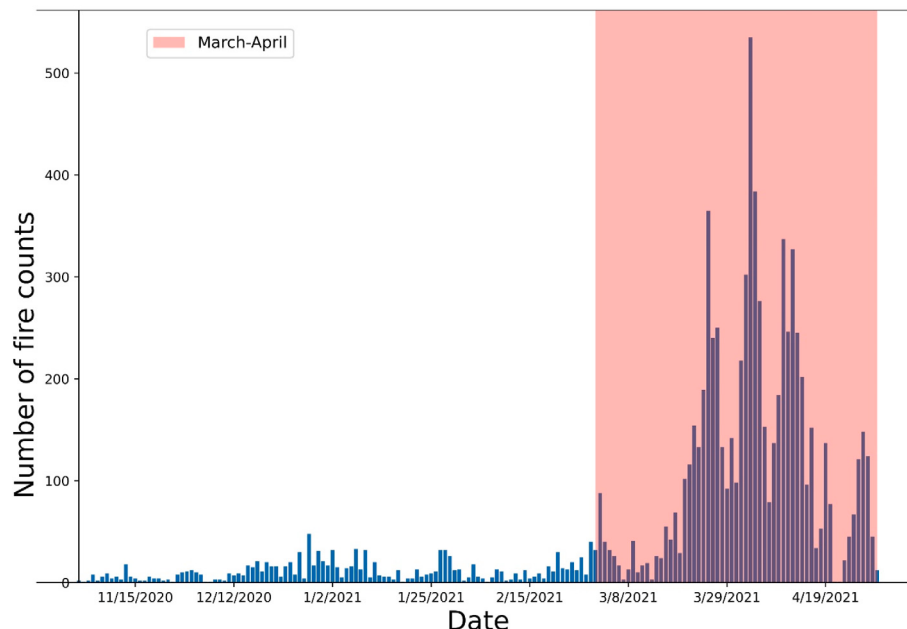


**Fig. 2.** Daily active fire count during November, 2020 to April, 2021 in our domain obtained from FIRMS.

From Fig. 2 we can see that there were fire events in November, which can influence the concentration of air pollutants in the month of December. Fig. 3 shows the trend of wildfire with contribution of fire on air pollutants. For time series analysis, coordinates of higher hotspot districts were used, which were Gorkha, Bajhang, Lamjung and Myagdi. Fig. 3 for the fire contribution is obtained using the difference between the concentrations with and without the wildfire (see Eq. (1)). Gorkha and Lamjung had a higher number of hotspots. So, greater contribution of fire to air pollutant concentration can be seen there in comparison to Myagdi and Bajhang. The main reason for that can be the high contribution from fire emission to pollutant concentration in the four districts. On December 18, peak fire contribution on pollutants was observed in Lamjung district with higher hotspots in that area. Similarly, Lamjung had higher contribution from fire on December 10, 14, and 26 as well. Gorkha and Lamjung had similar trends as they are located adjacent to each other. Link between increase in fire hotspots and increase in concentration of pollutants from wildfires was observed.

Similar study with the WRF-Chem has been carried out in North western region of India for the two consecutive fire events which had occurred in 24 April to 2 May of 2016 (first event) and 20 May to 30 May of 2018 (second event) (Yarragunta et al., 2020). Three parameters were taken into account for the determination of the effect of biomass burning in this study namely  $\text{NO}_x$ , CO, and  $\text{O}_3$ . In the study it was found that the CO was the highest emitted gas between these three followed by  $\text{O}_3$  and  $\text{NO}_x$ , in the first event the level of CO increased by 177 ppb<sub>v</sub>, while the  $\text{O}_3$  and  $\text{NO}_x$  increased by 13 ppb<sub>v</sub> and 2 ppb<sub>v</sub> respectively. Similarly, in the second event the CO increased by 118 ppb<sub>v</sub> while the  $\text{O}_3$  and the  $\text{NO}_x$  increased by 1 ppb<sub>v</sub> and 12 ppb<sub>v</sub> respectively.

According to Wiedinmyer et al. (2011) there is uncertainty in the estimation of gases like CO,  $\text{NO}_x$ , and  $\text{O}_3$ . The use of GLOBCOVER as land cover type in comparison to MODIS in the simulation process increased the forest fires by 70%. Similarly the emission of CO and NMVOCs were also 20% and 24% more with GLOBCOVER data set than the MODIS while simulating the emission for the regions of U.S., Mexico and Central America. Additionally, the determination of the level of uncertainty is complex due to the association of the uncertainty with classifications of land cover classes, detection of fire hotspots, the assumptions of the burned area, biomass loading, amount of fuel burned, and also the emission factors (Wiedinmyer et al., 2011).

### 3.2. Emission from satellite imagery

In a previous study it was found that only the modeling approach wasn't enough for the quantification of the air pollutants as the model output underestimated the level of air pollution in comparison to the satellite images and observations (Mahapatra et al., 2019). With the data of one year, it was found that the column density of  $\text{NO}_2$  obtained from the satellite images was in high correlation ( $R^2 = 0.72$ ) with the concentration obtained from the ground based stations (Zheng et al., 2019). Similarly, another study found that even the sparse data were useful in CO monitoring by the satellite imagery (Magro et al., 2021). In addition to this, the Sentinel imagery has also been used for studying the emission from the wildfire events in different countries of the world, namely Portugal (Magro et al., 2021), Canada (Alvarado et al., 2020), United States of America (Li et al., 2020), etc.

Hence, we opted to take into account the results from the satellite imagery along with the results from modeling for better understanding of the emission and its impact. With the satellite images, our results highlight the important changes between the time frames of the dry-winter to pre-monsoon period from November, 2020 to April, 2021. Comparative cartographic representations of the daily average of the mosaics of the tropospheric  $\text{NO}_2$ , and  $\text{SO}_2$  column number density (CND), Ultraviolet Absorbing Aerosol Index (UV-AAI),  $\text{O}_3$ , and trace gases like CO extracted from Copernicus Sentinel-5P imagery were drawn for a better comprehension of the spatial and temporal changes that had occurred across the country during the selected study period.

To evaluate the seasonal variation of wildfire impact on air quality, satellite-based observations of CO,  $\text{O}_3$ ,  $\text{SO}_2$ ,  $\text{NO}_2$ , and UV-AAI across winter (November–February) and pre-monsoon (March–April) seasons were analyzed. Distinct increases in pollutant levels were observed during March and April 2021, corresponding to peak wildfire activity (Fig. 4).

#### 3.2.1. Carbon monoxide

Apart from particulate matters, the CO emissions are found to be significantly high during wildfire events (Alves et al., 2011). The emission of CO is also of interest due to its severe impact on health of public. With an increase in the rate of CO in human blood, person may suffer at different levels, ranging from slight cardiovascular and neuro-behavioral alterations to unconsciousness and death at higher level of

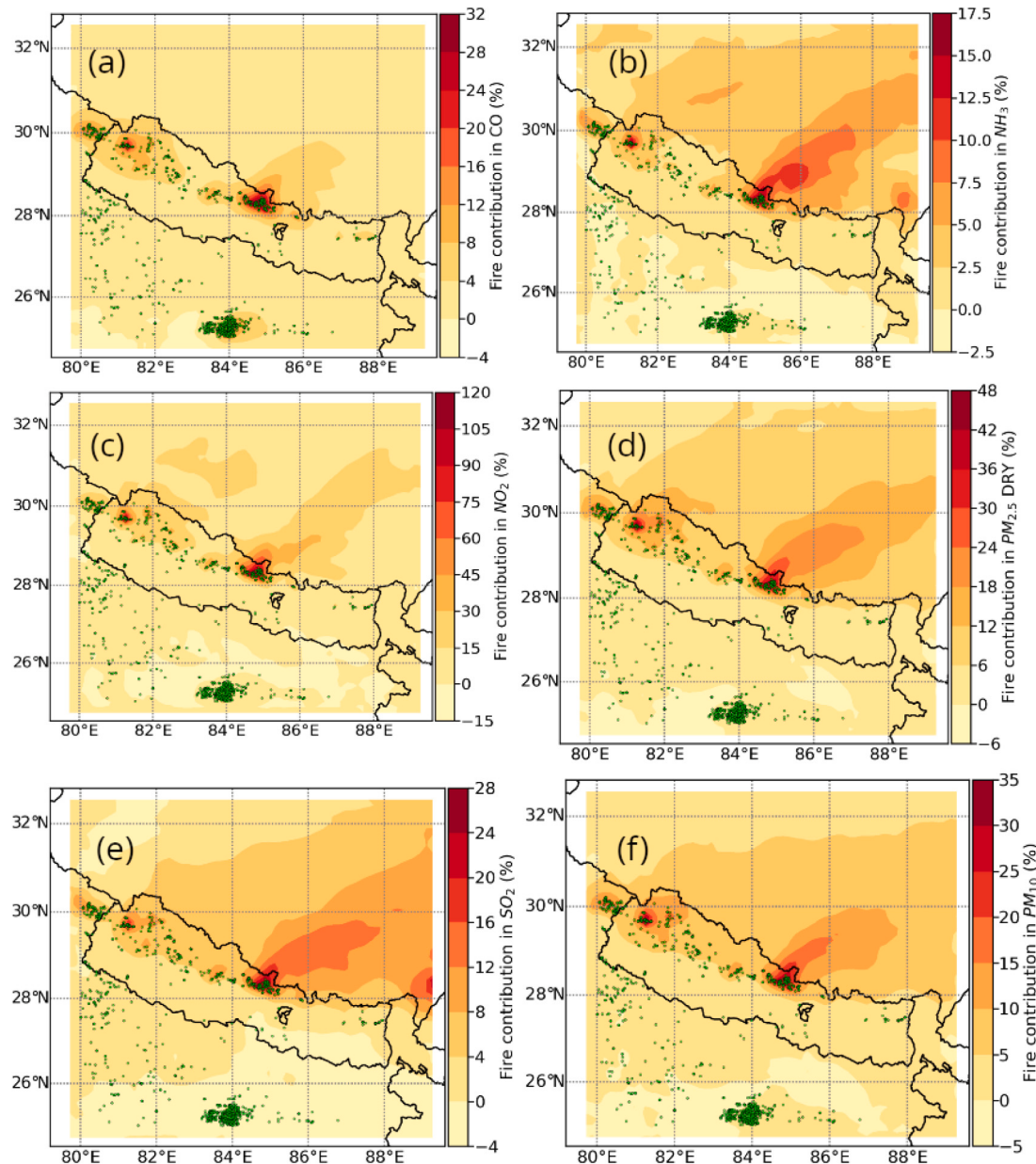


**Fig. 3.** Percentage contribution of wildfire on air pollutants (using Eq. (1)) in domain during December, 2020 and the hotspots of wildfires. (a) CO; (b) NH<sub>3</sub>; (c) NO<sub>2</sub>; (d) PM<sub>2.5</sub>; (e) SO<sub>2</sub>; (f) PM<sub>10</sub>. All data from WRF-Chem simulation.

concentrations (Raub et al., 2000). The distribution of CO is found to be high in the central regions of Nepal during the month of March, 2021 (Fig. 5). In comparison to other months, the CO concentration showed higher values in the months of March and April. This observation can be attributed to the seasonal changes in meteorological conditions and boundary layer dynamics, as well as the occurrence of forest fires. The trend of CO was observed to be increasing towards the central and western parts of Nepal from the southeastern part of Nepal (Fig. S4). The biomass burning and forest fires contribute towards an increase in the concentration of carbon monoxide during autumn and pre-monsoon.

The monthly mean CO column number density in Nepal was moderately high for November to February and maximum average ( $0.04211 \text{ mol m}^{-2}$ ) during March–April (Fig. 4). The CO-column number density concentration for the districts lying in the Terai belt (southern part) of Nepal increased tremendously in March and April, in comparison to November–February, 2020/2021. For March–April months of 2021, the CO-column number density demonstrated higher values, while a marginal decline was observed during the dry winter season for 2020.

### 3.2.2. Ozone

The Ozone ( $\text{O}_3$ ) column number density was found higher for the southern part of the country i.e. Terai region compared to the northern part, with maximum during November–December, 2020 and minimum during February (Fig. S5). We notice the gradual increase in the column number density of ozone in the month of March–April, 2021, which can be explained by the emission contributed by the fire emission of the pre-monsoon season. The seasonal average ozone concentration was more from March to April and increased during the winter month i.e. January 2021 (Fig. 4).

The pattern of  $\text{O}_3$  over the months suggests that the concentration of  $\text{O}_3$  is higher during the pre-monsoon season. The high photochemical formation of  $\text{O}_3$  can be partly attributed to the increase in surface temperature from wildfires.

### 3.2.3. Ultraviolet Aerosol Index (UVAI)

The UV-AAI provides an idea regarding the presence of absorbing particles. The UV-AAI distinguishes the spectral values due to the

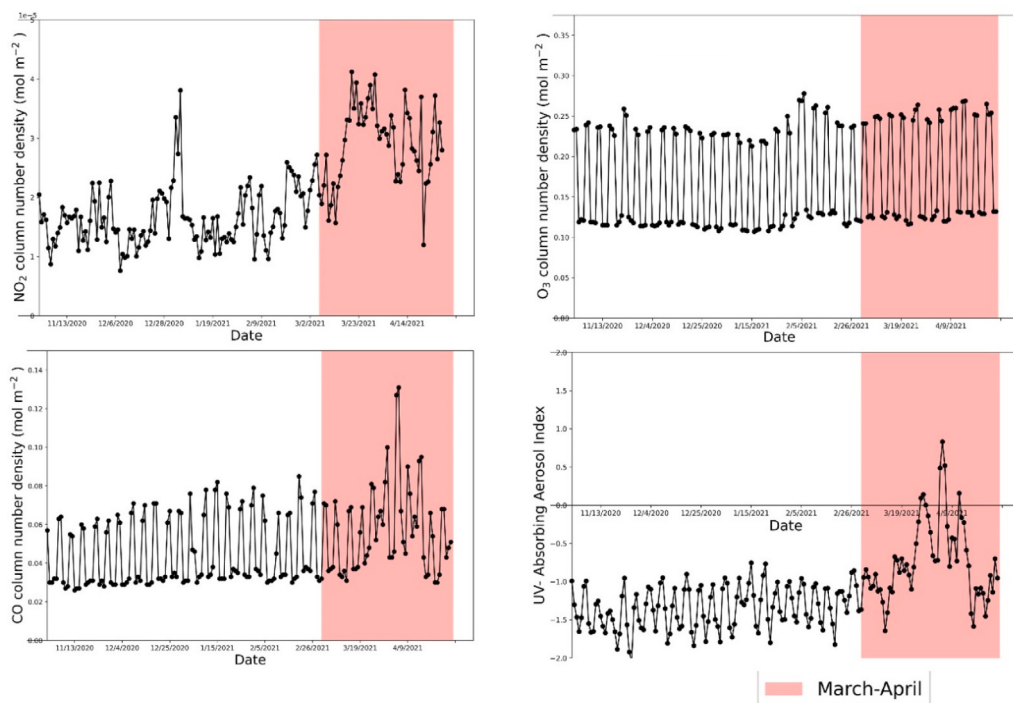


**Fig. 4.** Change in air pollution from November, 2020 to April, 2021.  
Source: Sentinel-5P.

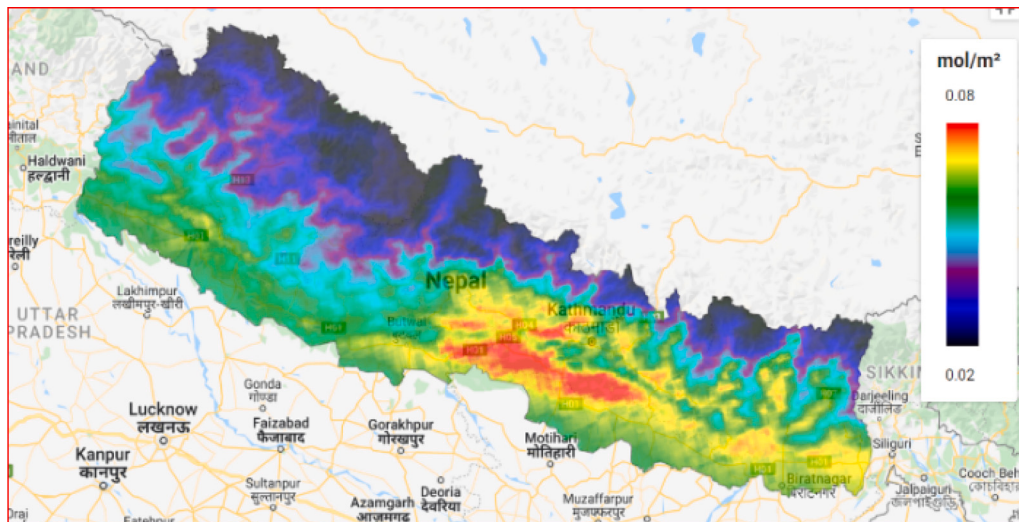


**Fig. 5.** Cartographic representations of the CO column number density of March, 2021 over Nepal.  
Source: Sentinel-5P.

absorption by the aerosol from the Rayleigh scattering, reflection from surfaces and also due to the absorption of trace gases (Torres et al., 1998). The value of UV-AAI ranges from negative to positive values. The presence of absorbing aerosols results in the positive value of UV-AAI, while the presence of non-absorbing aerosol results in the negative values of UV-AAI and in ideal case the UV-AAI is zero indicating there is no absorbing or scattering particles in the atmosphere (Hammer et al., 2016).

The Ultraviolet Absorbing Aerosol Index (UV-AAI) values were generally negative for Nepal except for the marginally positive and higher value along north-western Nepal around the mid-hills and Mahabharata range region in the month of pre-monsoon season i.e. March–April, 2021 as shown in Fig. S6. The increase in absorbing aerosols in the upper atmosphere over far western mid hilly and southern Terai region in

March–April 2020; and a prominent decrease in January and February 2021 can be seen. The aerosol index was significantly greater with an average absorbing aerosol index value to be  $-0.7356$  in pre-monsoon months than in the dry winter season with an average UV-AAI value of  $-1.3870$  as shown in Fig. 4.

The UV-absorbing aerosol index in the first four months of the study period demonstrated a reduction in absorbing aerosols. Wildfires emit large concentrations of particulate matter along with trace gases. The higher distribution of positive daily values of the UV-AAI in April 2021 showed the presence of absorbing aerosols in the atmosphere over the country since fire counts in March and April 2021 were maximum. The wildfire events in southwestern, mid-hills, and Terai region release strong absorbing aerosols into the atmosphere.

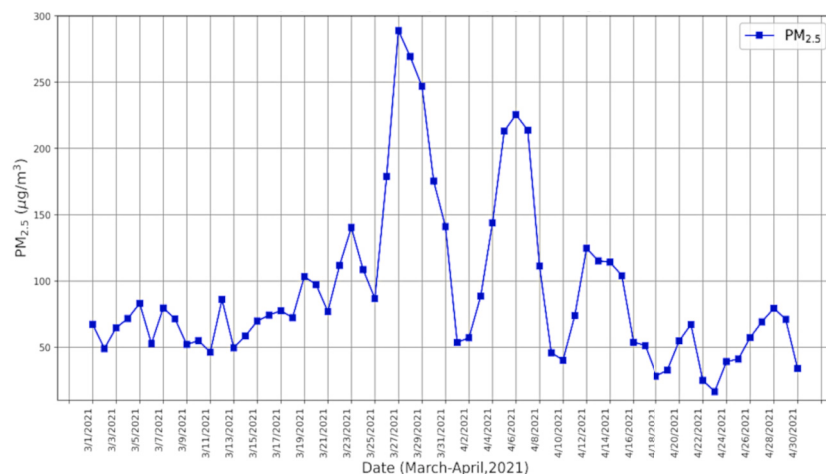


**Fig. 6.** PM<sub>2.5</sub> concentration of US Embassy, Phora-Durbar station for March and April 2021.

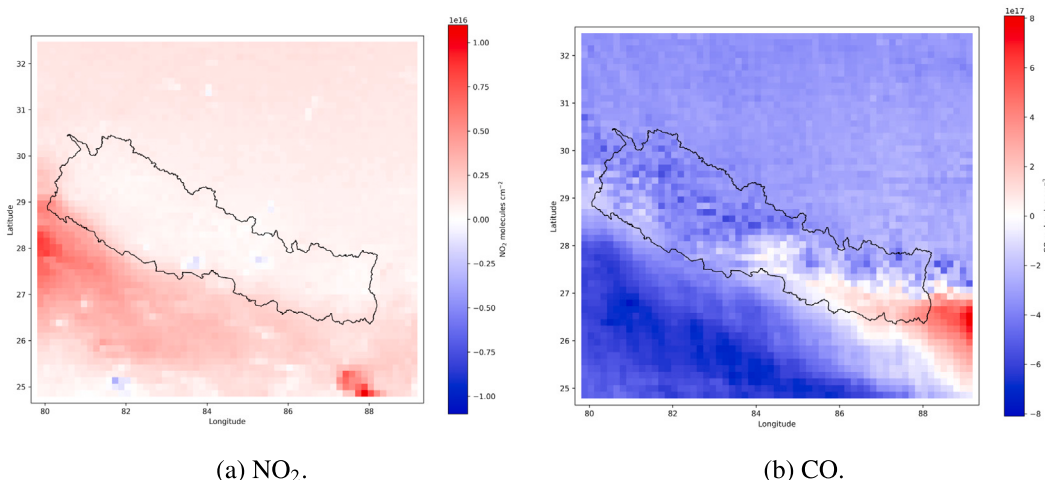


**Fig. 7.** Difference plot of tropospheric column concentration (WRF-Chem – Sentinel-5P) for December 2020.

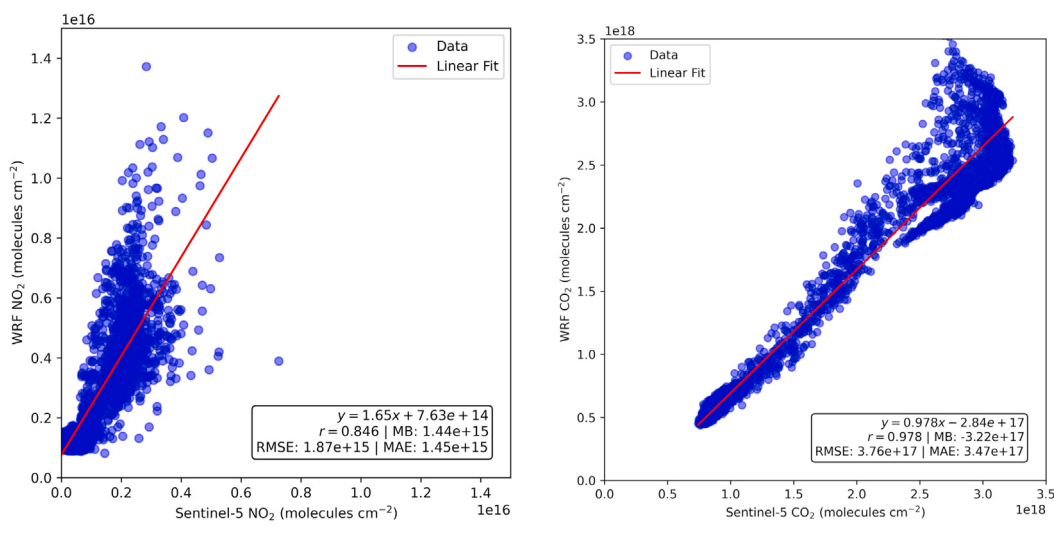


**Fig. 8.** Scatter plot of tropospheric column concentration from all grid points for December 2020.

### 3.2.4. SO<sub>2</sub>

The variation in SO<sub>2</sub> column number density was minimum in starting of November, 2020 and gradually increased in December and March month over Nepal (Fig. S9). Also, the Terai and Hilly regions of Nepal demonstrated higher SO<sub>2</sub> concentration from November to April compared to Himalayan regions. Concentration of SO<sub>2</sub> increased in the pre-monsoon period i.e. March in Terai and Hilly regions (Fig. S8). Average SO<sub>2</sub> column number density of December ( $4.6 \times 10^{-5}$  mol m<sup>-2</sup>), March ( $1.3338 \times 10^{-5}$  mol m<sup>-2</sup>) and April ( $1.24 \times 10^{-4}$  mol m<sup>-2</sup>) was high because the number of hotspots of fire was 513, 2600, and 4760, respectively.

In Nepal, the emission of SO<sub>2</sub> has increased over the years, aggravating air pollution problems. The SO<sub>2</sub> column number density showed seasonal variation during the winter and pre-monsoon season, due to precipitation and dilution by transport of cleaner air. The forest fire induced by human activities was considerably high during the study period. December 2020 and April 2021 has recorded a substantial and higher level of SO<sub>2</sub> emission (Fig. S9), which can be attributed to the wildfires in Nepal. A substantial decrease in SO<sub>2</sub> level in January and February, 2020 could be seen.

### 3.2.5. NO<sub>2</sub>

The maps of NO<sub>2</sub> from November, 2020 to April, 2021 (Fig. S7) show no substantial change between 2020 and 2021, except for month of March and April, as it maintains moderate values on large areas across the country. As for two months i.e. March and April in Nepal, increase in NO<sub>2</sub> can be characterized by the occurrence of forest fires throughout the country, mainly in the major cities of southern Terai region. The wind can disperse the NO<sub>2</sub> pollutants in less than 30 min (Richmond-Bryant et al., 2018) as the maximum wind speed was 31.1 mph (data obtained from Department of Hydrology and Meteorological (DHM), Nepal) in the month of April.

From Fig. 4, we can notice that NO<sub>2</sub> column number density increased from mid-week of December 2020 and gradually spiked to the highest NO<sub>2</sub> CND in the month of January, March and April 2021. This can be explained by forest fire in the winter and pre-monsoon period. Due to wildfire in the winter period, soil humidity increases which leads to increase in biogenic emission too (Pommier et al., 2018).

### 3.3. Ground station for PM<sub>2.5</sub>

Fig. 6 shows the time-series graph of ground station PM<sub>2.5</sub> concentration data of US-Embassy, Phora Durbar Kathmandu for March and April. The PM<sub>2.5</sub> graph shows spikes in the month of March–April, which can be attributed to the emissions due to wildfire. Three peak PM concentrations were observed from 20 March to 16 April. We can see that the peak PM<sub>2.5</sub> concentration was measured to be 270 µg m<sup>-3</sup>. This shows that air quality was highly degraded during that time in Kathmandu as PM<sub>2.5</sub> concentration exceeds 24-h average WHO (PM<sub>2.5</sub> 15 µg m<sup>-3</sup>) guidelines and NAAQS (PM<sub>2.5</sub> 40 µg m<sup>-3</sup>) limits. Fire count data from Fig. 2 showed a similar pattern with PM<sub>2.5</sub> concentration for the period. Along with the increase in fire count, PM<sub>2.5</sub> concentrations had also increased and along with the decrease in fire count, PM<sub>2.5</sub> concentration had also decreased in a similar period. From both WRF-Chem results and Sentinel-5P satellite data, contribution of wildfire on air quality is evident. So we can say that wildfire had influenced air quality all over Nepal including the most populated city of Nepal, Kathmandu.

### 3.4. Comparison of results from WRF-Chem and Sentinel-5P

The comparison of NO<sub>2</sub> and CO concentrations between WRF-Chem and Sentinel-5P demonstrated a generally strong agreement. Among the evaluated metrics, the Pearson correlation coefficient (r) was found to be 0.846 for NO<sub>2</sub> and 0.978 for CO, indicating a stronger correlation mainly for the carbon monoxide.

The mean bias (MB) was calculated as  $1.44 \times 10^{15}$  molecules cm<sup>-2</sup> for NO<sub>2</sub> and  $-3.22 \times 10^{17}$  molecules cm<sup>-2</sup> for CO. This suggests that WRF overestimated NO<sub>2</sub> concentrations and underestimated CO concentrations compared to Sentinel-5P observations. Furthermore, for NO<sub>2</sub>, the root mean squared error (RMSE) and mean absolute error (MAE) were  $1.87 \times 10^{15}$  molecules cm<sup>-2</sup> and  $1.45 \times 10^{15}$  molecules cm<sup>-2</sup>, respectively (Fig. 7). In the case of CO, the RMSE and MAE were  $3.76 \times 10^{17}$  molecules cm<sup>-2</sup> and  $3.47 \times 10^{17}$  molecules cm<sup>-2</sup> (Fig. 8).

## 4. Conclusion

We utilized WRF-Chem to better understand the impact of wildfire events that occurred between November 2020 and April 2021. Hotspots were located more in Lesser Himalayan and mid-hills region, but the occurrence was seen in almost every district of Nepal. Similarly, in December, we found the contribution of wildfire in increasing the pollutants level was high, with 120% increase for NO<sub>2</sub>, followed by 48% for PM<sub>2.5</sub>, 35% for PM<sub>10</sub>, and 32% for CO, 28% for SO<sub>2</sub> and 17.5% for NH<sub>3</sub>. Likewise, the images from Sentinel-5 revealed that, with the increase in the fire counts during March and April 2021, the pollutant levels increased. The maximum UV-AAI was 0.8315, and CO and NO<sub>2</sub> column number densities were 0.067 mol m<sup>-2</sup> and  $4.1204 \times 10^{-5}$  mol m<sup>-2</sup> respectively. A similar trend observed in the ground station data in the US embassy in Kathmandu supported our findings from simulation and remote sensing.

Previous studies also demonstrate the significant impact of wildfires on air quality. Studies from North America (Shi et al., 2019), Europe (Magro et al., 2021), and Asia (Murmu et al., 2022) have shown that wildfire events lead to sharp increases in atmospheric pollutants and pose serious health risks. Research in the Himalayan region also highlights the transboundary transport of wildfire-related pollutants, emphasizing the broader regional consequences (Xu et al., 2018). In Nepal, recent studies confirm that wildfire smoke significantly degrades urban air quality (Khadgi et al., 2024; Kuikel et al., 2024).

The government of Nepal has developed the Forest Fire Management Strategy 2010 and implemented awareness-raising programs to prevent and control forest fires. They have allocated public finance for forest fire management and established a forest fire control room to track incidents. Additionally, the government promotes sustainable forest management practices and has embraced the REDD+ mechanism to conserve forests and control wildfires (Pandey et al., 2022). Also, Nepal Disaster Risk Reduction Portal reports fire incidents which includes location of fire, date, deaths and estimated loss for awareness and to strategize action plan.

However, governmental efforts to mitigate wildfire impacts remain limited. There is an urgent need for stronger policies, improved enforcement, and regional cooperation. This study underscores the importance of integrating atmospheric modeling and satellite observations to support evidence-based decision-making and enhance wildfire response strategies.

## CRediT authorship contribution statement

**Kundan Lal Shrestha:** Writing – original draft, Software, Methodology, Formal analysis, Conceptualization. **Aakriti Gyawali:** Writing – original draft, Validation, Data curation. **Sabina Gyawali:** Writing – original draft, Visualization, Validation. **Prayon Joshi:** Writing – original draft, Visualization, Software. **Subodh Sharma:** Writing – review & editing, Supervision, Project administration, Funding acquisition.

## Declaration of competing interest

The authors declare that they have no known competing financial interests or personal relationships that could have appeared to influence the work reported in this paper.

## Acknowledgment

The authors would like to acknowledge the support of UKRI-GCRF-South Asian Nitrogen Hub (NE/S009019/1).

## Appendix A. Supplementary data

Supplementary material related to this article can be found online at <https://doi.org/10.1016/j.envpol.2025.126545>.

## Data availability

Data will be made available on request.

## References

- Alvarado, L.M.A., Richter, A., Vrekoussis, M., Hilboll, A., Kalisz Hedegaard, A.B., Schnieising, O., Burrows, J.P., 2020. Unexpected long-range transport of glyoxal and formaldehyde observed from the copernicus sentinel-5 precursor satellite during the 2018 Canadian wildfires. *Atmos. Chem. Phys.* 20 (4), 2057–2072. <http://dx.doi.org/10.5194/acp-20-2057-2020>.
- Alves, C.A., Vicente, A., Monteiro, C., Gonçalves, C., Evtyugina, M., Pio, C., 2011. Emission of trace gases and organic components in smoke particles from a wildfire in a mixed-evergreen forest in Portugal. *Sci. Total Environ.* 409 (8), 1466–1475. <http://dx.doi.org/10.1016/j.scitotenv.2010.12.025>.
- Bhattarai, N., Dahal, S., Thapa, S., Pradhananga, S., Karky, B.S., Rawat, R.S., Windhorst, K., Watanabe, T., Thapa, R.B., Avtar, R., 2022. Forest fire in the hindu kush Himalayas: A major challenge for climate action. *J. For. Livelihood* 21 (1), 14–31. <http://dx.doi.org/10.3126/jfl.v21i1.56576>, URL: <https://www.nepjol.info/index.php/JFL/article/view/56576>.
- Bhujel, K.B., Maskay-Byanju, R., Gautam, A.P., 2017. Wildfire dynamics in nepal from 2000–2016. *Nepal J. Environ. Sci.* 5, 1–8. <http://dx.doi.org/10.3126/njes.v5i0.22709>.
- Bhujel, K.B., Maskay Byanju, R., Gautam, A.P., Sapkota, R.P., Khadka, U.R., 2020. Fire-induced carbon emissions from tropical mixed broad-leaved forests of the Terai-Siwalik region, central Nepal. *J. For. Res.* 32 (6), 2557–2565. <http://dx.doi.org/10.1007/s11676-020-01256-x>.
- Bista, R., 2019. Trend and forecasting analysis on climate variability: A case of nepal. *J. Adv. Civ. Environ. Eng.* 6 (1), 1–6, URL: <https://mpra.ub.uni-muenchen.de/98788/>. MPRA Paper No. 98788.
- Crippa, P., Castruccio, S., Archer-Nicholls, S., Lebron, G.B., Kuwata, M., Thota, A., Sumin, S., Butt, E., Wiedinmyer, C., Spracklen, D.V., 2016. Population exposure to hazardous air quality due to the 2015 fires in equatorial Asia. *Sci. Rep.* 6 (1), 1–9. <http://dx.doi.org/10.1038/srep37074>.
- DHM, 2021. Winter (december 2020 - february 2021) rainfall monitoring. URL: [https://www.dhm.gov.np/uploads/dhm/climateService/Winter\\_Precipitation\\_monitoring\\_28th\\_february\\_2021.pdf](https://www.dhm.gov.np/uploads/dhm/climateService/Winter_Precipitation_monitoring_28th_february_2021.pdf).
- Fatholah, S.N., Gu, Y., Liu, M., Ma, L., Chen, Y., Li, J., 2020. Estimating PM2.5 concentrations in British Columbia, Canada during wildfire season using satellite optical data. *ISPRS Ann. Photogramm. Remote. Sens. Spat. Inf. Sci.* V-1-2020, 71–79. <http://dx.doi.org/10.5194/isprs-annals-v-1-2020-71-2020>.
- Giglio, L., Schroeder, W., Justice, C.O., 2016. The collection 6 MODIS active fire detection algorithm and fire products. *Remote Sens. Environ.* 178, 31–41. <http://dx.doi.org/10.1016/j.rse.2016.02.054>.
- Grell, G., Freitas, S.R., Stuefer, M., Fast, J., 2011. Inclusion of biomass burning in WRF-Chem: impact of wildfires on weather forecasts. *Atmos. Chem. Phys.* 11 (11), 5289–5303. <http://dx.doi.org/10.5194/acp-11-5289-2011>.
- Guenther, A., Karl, T., Harley, P., Wiedinmyer, C., Palmer, P.I., Geron, C., 2006. Estimates of global terrestrial isoprene emissions using MEGAN (model of emissions of gases and aerosols from nature). *Atmos. Chem. Phys.* 6 (11), 3181–3210. <http://dx.doi.org/10.5194/acp-6-3181-2006>, URL: <https://acp.copernicus.org/articles/6/3181/2006/>.
- Hammer, M.S., Martin, R.V., van Donkelaar, A., Buchard, V., Torres, O., Ridley, D.A., Spurr, R.J.D., 2016. Interpreting the ultraviolet aerosol index observed with the OMI satellite instrument to understand absorption by organic aerosols: implications for atmospheric oxidation and direct radiative effects. *Atmos. Chem. Phys.* 16 (4), 2507–2523. <http://dx.doi.org/10.5194/acp-16-2507-2016>.
- iQAir, 2021. Air quality in nepal. URL: <https://www.iqair.com/nepal>.
- Janwal, N., 2021. Nepal's forest fires under control, but peak wildfire season has just begun. URL: <https://en.gaoconnection.com/reportage/nepal-forest-fire-kathmandu-wildfire-climate-change-air-pollution-himalayas/>.
- Janssens-Maenhout, G., Dentener, F., Van Aardenne, J., Monni, S., Pagliari, V., Orlandini, L., Klimont, Z., Kurokawa, J., Akimoto, H., Ohara, T., Wankmüller, R., Battye, B., Grano, D., Zuber, A., Keating, T., 2012. EDGAR-HTAP: A Harmonized Gridded Air Pollution Emission Dataset Based on National Inventories. Publications Office of the European Union, Luxembourg, [http://dx.doi.org/10.2788/14069\(print\),10.2788/14102\(online\)](http://dx.doi.org/10.2788/14069(print),10.2788/14102(online)).
- Jena, C., Ghude, S.D., Pfister, G., Chate, D., Kumar, R., Beig, G., Surendran, D.E., Fadnavis, S., Lal, D., 2015. Influence of springtime biomass burning in south Asia on regional ozone (O<sub>3</sub>): A model based case study. *Atmos. Environ.* 100, 37–47. <http://dx.doi.org/10.1016/j.atmosenv.2014.10.027>.
- Karki, R., Hasson, S.U., Schickhoff, U., Scholten, T., Böhner, J., 2017. Rising precipitation extremes across Nepal. *Climate* 5 (1), 4. <http://dx.doi.org/10.3390/cli5010004>, URL: <https://www.mdpi.com/2225-1154/5/1/4>. Number: 1 Publisher: Multidisciplinary Digital Publishing Institute.
- Khadgi, J., Kafle, K., Thapa, G., Khaitu, S., Sarangi, C., Cohen, D., Kafle, H., 2024. Concentration of particulate matter and atmospheric pollutants in the residential area of Kathmandu Valley: A case study of March-April 2021 forest fire events. *Environ. Pollut.* 363, 125280. <http://dx.doi.org/10.1016/j.envpol.2024.125280>, URL: <https://linkinghub.elsevier.com/retrieve/pii/S0269749124019973>.
- Kuikel, S., Pokhrel, B., Bhattacharai, N., 2024. The effect of wildfires on air quality in Kathmandu, Nepal. *Environ. Adv.* 15, 100493. <http://dx.doi.org/10.1016/j.envadv.2024.100493>, URL: <https://linkinghub.elsevier.com/retrieve/pii/S2666765724000115>.
- Lazaridis, M., Latos, M., Aleksandropoulou, V., Hov, Ø., Papayannis, A., Tørseth, K., 2008. Contribution of forest fire emissions to atmospheric pollution in Greece. *Air Qual. Atmos. Heal.* 1 (3), 143–158. <http://dx.doi.org/10.1007/s11869-008-0020-0>.
- Li, F., Zhang, X., Kondragunta, S., Lu, X., 2020. An evaluation of advanced baseline imager fire radiative power based wildfire emissions using carbon monoxide observed by the tropospheric monitoring instrument across the conterminous United States. *Environ. Res. Lett.* 15 (9), 094049. <http://dx.doi.org/10.1088/1748-9326/ab9d3a>.
- Magro, C., Nunes, L., Gonçalves, O., Neng, N., Nogueira, J., Rego, F., Vieira, P., 2021. Atmospheric trends of CO and CH<sub>4</sub> from extreme wildfires in Portugal using sentinel-5P TROPOMI level-2 data. *Fire* 4 (2), 25. <http://dx.doi.org/10.3390/fire4020025>, URL: <https://www.mdpi.com/2571-6255/4/2/25>. Number: 2 Publisher: Multidisciplinary Digital Publishing Institute.
- Mahapatra, P.S., Puppala, S.P., Adhikary, B., Shrestha, K.L., Dawadi, D.P., Paudel, S.P., Panday, A.K., 2019. Air quality trends of the kathmandu valley: A satellite, observation and modeling perspective. *Atmos. Environ.* 201 (January), 334–347. <http://dx.doi.org/10.1016/j.atmosenv.2018.12.043>.
- McClure, C.D., Jaffe, D.A., 2018. US particulate matter air quality improves except in wildfire-prone areas. *Proc. Natl. Acad. Sci.* 115 (31), 7901–7906. <http://dx.doi.org/10.1073/pnas.1804353115>.
- Menon, S., Denman, K.L., Brasseur, G., Chidthaisong, A., Ciais, P., Cox, P.M., Dickinson, R.E., Hauglustaine, D., Heinze, C., Holland, E., Jacob, D., Lohmann, U., Ramachandran, S., Leite da Silva Dias, P., Wofsy, S.C., Zhang, X., 2007. Couplings Between Changes in the Climate System and Biogeochemistry. United States, arXiv:SponsorOrg.:EnvironmentalEnergyTechnologiesDivision. URL: <https://www.osti.gov/servlets/purl/934721>.
- Mues, A., Lauer, A., Lupascu, A., Rupakheti, M., Kuik, F., Lawrence, M.G., 2017. Air quality in the kathmandu valley: WRF and WRF-Chem simulations of meteorology and black carbon concentrations. *Geosci. Model. Dev. Discuss.* 17, <http://dx.doi.org/10.5194/gmd-2017-224>.
- Murmu, M., Roy, A., Karnataka, H.C., Chauhan, P., 2022. Impact of forest fire emissions on air quality over Western Himalaya Region. *Int. Arch. Photogramm. Remote. Sens. Spat. Inf. Sci.* XLIII-B3-2022, 1153–1160. <http://dx.doi.org/10.5194/isprs-archives-xliii-b3-2022-1153-2022>.
- NPHC, 2021. National population and housing census 2021. URL: <https://censusnepal.cbs.gov.np/results>.
- Pandey, H.P., Pokhrel, N.P., Thapa, P., Paudel, N.S., Maraseni, T.N., 2022. Status and practical implications of forest fire management in nepal. *J. For. Livelihood* 21 (1), 32–45. <http://dx.doi.org/10.3126/jfl.v21i1.56583>.
- Parajuli, A., Chand, D., Rayamajhi, B., Khanal, R., Baral, S., Malla, Y., Paudel, S., 2015. Spatial and temporal distribution of forest fires in Nepal. In: XIV World Forestry Congress. Durban, South Africa.
- Pommier, M., Fagerli, H., Gauss, M., Simpson, D., Sharma, S., Sinha, V., Ghude, S.D., Landgren, O., Nyiri, A., Wind, P., 2018. Impact of regional climate change and future emission scenarios on surface O<sub>3</sub> and PM<sub>2.5</sub> over India. *Atmos. Chem. Phys.* 18 (1), 103–127. <http://dx.doi.org/10.5194/acp-18-103-2018>, URL: <https://acp.copernicus.org/articles/18/103/2018/>.
- Raub, J.A., Mathieu-Nolf, M., Hampson, N.B., Thom, S.R., 2000. Carbon monoxide poisoning – a public health perspective. *Toxicology* 145 (1), 1–14. [http://dx.doi.org/10.1016/s0300-483x\(99\)00217-6](http://dx.doi.org/10.1016/s0300-483x(99)00217-6).
- Reuters, 2021. Nepal chokes on smoke, ash as wildfires rage. URL: <https://thehindalayantimes.com/nepal/nepal-chokes-on-smoke-ash-as-wildfires-rage>.
- Richmond-Bryant, J., Snyder, M., Owen, R., Kimbrough, S., 2018. Factors associated with NO<sub>2</sub> and NO<sub>x</sub> concentration gradients near a highway. *Atmos. Environ.* 174, 214–226. <http://dx.doi.org/10.1016/j.atmosenv.2017.11.026>, URL: <https://linkinghub.elsevier.com/retrieve/pii/S1352231017307719>.
- Sadaravate, P., Rupakheti, M., Bhave, P., Shakya, K., Lawrence, M., 2019. Nepal emission inventory - part I: Technologies and combustion sources (NEEMI-Tech) for 2001–2016. *Atmos. Chem. Phys.* 19 (20), 12953–12973. <http://dx.doi.org/10.5194/acp-19-12953-2019>.

- Shi, H., Jiang, Z., Zhao, B., Li, Z., Chen, Y., Gu, Y., Jiang, J.H., Lee, M., Liou, K.-N., Neu, J.L., Payne, V.H., Su, H., Wang, Y., Witek, M., Worden, J., 2019. Modeling study of the air quality impact of record-breaking southern California wildfires in December 2017. *J. Geophys. Res.: Atmos.* 124 (12), 6554–6570. <http://dx.doi.org/10.1029/2019jd030472>.
- Torres, O., Bhartia, P.K., Herman, J.R., Ahmad, Z., Gleason, J., 1998. Derivation of aerosol properties from satellite measurements of backscattered ultraviolet radiation: Theoretical basis. *J. Geophys. Res.: Atmos.* 103 (D14), 17099–17110. <http://dx.doi.org/10.1029/98jd00900>.
- Ukhov, A., Mostamandi, S., Krotkov, N., Flemming, J., da Silva, A., Li, C., Fioletov, V., McLinden, C., Anisimov, A., Alshehri, Y.M., Stenchikov, G., 2020. Study of SO<sub>2</sub> pollution in the middle east using MERRA-2, CAMS data assimilation products, and high-resolution WRF-Chem simulations. *J. Geophys. Res.: Atmos.* 125 (6), e2019JD031993. <http://dx.doi.org/10.1029/2019jd031993>.
- Val Martín, M., Honrath, R.E., Owen, R.C., Pfister, G., Fialho, P., Barata, F., 2006. Significant enhancements of nitrogen oxides, black carbon, and ozone in the North Atlantic lower free troposphere resulting from North American boreal wildfires. *J. Geophys. Res.: Atmos.* 111 (D23), 1–17. <http://dx.doi.org/10.1029/2006jd007530>.
- Wiedinmyer, C., Akagi, S.K., Yokelson, R.J., Emmons, L.K., Al-Saadi, J.A., Orlando, J.J., Soja, A.J., 2011. The fire INventory from NCAR (FINN): a high resolution global model to estimate the emissions from open burning. *Geosci. Model. Dev.* 4 (3), 625–641. <http://dx.doi.org/10.5194/gmd-4-625-2011>.
- Xu, R., Tie, X., Li, G., Zhao, S., Cao, J., Feng, T., Long, X., 2018. Effect of biomass burning on black carbon (BC) in South Asia and Tibetan Plateau: The analysis of WRF-Chem modeling. *Sci. Total Environ.* 645, 901–912. <http://dx.doi.org/10.1016/j.scitotenv.2018.07.165>.
- Yang, K., Guyennon, N., Ouyang, L., Tian, L., Tartari, G., Salerno, F., 2017. Impact of summer monsoon on the elevation-dependence of meteorological variables in the south of central Himalaya. *Int. J. Climatol.* 38 (4), 1748–1759. <http://dx.doi.org/10.1002/joc.5293>.
- Yarragunta, Y., Francis, D., Fonseca, R., Nelli, N., 2025. Evaluation of the WRF-Chem performance for the air pollutants over the United Arab Emirates. *Atmos. Chem. Phys.* 25 (3), 1685–1709. <http://dx.doi.org/10.5194/acp-25-1685-2025>.
- Yarragunta, Y., Srivastava, S., Mitra, D., Chandola, H.C., 2020. Influence of forest fire episodes on the distribution of gaseous air pollutants over Uttarakhand, India. *GIScience Remote. Sens.* 57 (2), 190–206. <http://dx.doi.org/10.1080/15481603.2020.1712100>.
- Zheng, Z., Yang, Z., Wu, Z., Marinello, F., 2019. Spatial variation of NO<sub>2</sub> and its impact factors in China: An application of Sentinel-5P products. *Remote. Sens.* 11 (16), 1939. <http://dx.doi.org/10.3390/rs11161939>.
- Zhu, Q., Liu, Y., Jia, R., Hua, S., Shao, T., Wang, B., 2018. A numerical simulation study on the impact of smoke aerosols from Russian forest fires on the air pollution over Asia. *Atmos. Environ.* 182, <http://dx.doi.org/10.1016/j.atmosenv.2018.03.052>.